OBSERVATIONS AND MODELING OF SLUSHFLOWS - ATIGUN PASS, ALASKA

David Hamre[1*], Lars Blatny[2,3,4], Johan Gaume[2,3,4], Peter Gauer[5], and Art Mears[6]

[1] David Hamre and Associates, LL, Alaska, USA
[2] Institute for Geotechnical Engineering, ETH Zurich, Switzerland
[3] Institute for Snow and Avalanche Research SLF, Davos, Switzerland
[4] Climate Change, Extremes, and Natural Hazards in Alpine Regions Research Center CERC, Davos, Switzerland
[5] Norwegian Geotechnical Institute, Oslo, Norway
[6] Arthur Mears P.E. Inc,

ABSTRACT: Slushflow consists of a mixture of snow, water, and ice and often entrain debris or sediments. The high mobility and high density of the flows make them a considerable natural hazard, endangering settlements and line infrastructures. They are primarily associated with higher latitudes, e.g., Norway, Iceland, or Alaska, but they have been reported in many other countries, e.g. from the Alps. In this paper, we discuss a number of slushflow events near Atigun Pass, Alaska, which were well documented in a study for the Alyeska Pipeline Service Company (APSC) in 1982. This information has been privately held and is now being released for research purposes. This paper describes these observations, and we apply modeling techniques to the described flows. We specifically consider both depth-averaged and depth-resolved numerical methods with viscoplastic and elasto-viscoplastic rheological models. These developments can help hazard mapping practitioners better account for the hazards originating from slushflows in the future.

KEYWORDS: slushflow, observations, numerical modeling

1. INTRODUCTION

Slushflows can be classified as fast moving mixtures of snow and water, which often erode and entrain surface sediments (Hestnes and Jaedicke, 2018). Typically, the water content by volume fraction is considerably larger than 15%. These flows have been previously reported, primarily in the Arctic, but have also been observed in other countries worldwide. They have resulted in many disaster events and caused fatalities. e.g., in both Iceland (Tomasson and Hestnes, 1999) and Norway (Hestnes et al., 2011, 2012) (See Figure 1).

Figure 1: Village impacts in Norway from slushflow (from Hestnes et al., 2012, Photo: W. Bjerkmo Sokjosen)

These events demonstrate the risks associated with locating facilities in slushflow paths. As their occurrence and release are poorly understood, it is relatively easy to overlook the presence of slushflow risk.

Previous work has focused on case studies and on identifying different types of slushflow behaviors and potential release areas (Hestnes, 1998; Hestnes and Kristensen, 2010; Hestnes et al., 2012 and reference therein). A set of common terms has been agreed to for describing the mass movement of very saturated snow (Onesti, 1995). We can classify all the Atigun Pass events as a “Release in Drainage Channels and Basins” and use the term slushflow to define them. Almost no dynamic modeling of slushflow behavior exists.

In Alaska, slushflows primarily occur in the Brooks Range north of the Arctic Circle. In the early 1980s, original research into slushflow behavior was conducted for the Alyeska Pipeline Service Company (APSC). Potential pipeline stability issues due to the threat of avalanches and slushflows prompted this analysis. Little was known about slushflows at the time. The research was conducted during the 1981 and 1982 seasons, with an internal report issued at the end of the study. While preliminary results were shared with the larger avalanche community in an abstract (Mears, 1982), the bulk of gathered observations have remained unreported until now.

Another factor enabling this work is the improved capability of modeling flow behaviors. Due to the inherent complexity caused by their transitional behavior between snow avalanches, fluvial mass transport, and debris flows, little attention has been paid to slushflow modeling. Only a few attempts have been made at specific slushflows models (Bozhinskiy et al.,1998; Gauer, 2004; Palsson et al., 2019). Otherwise, Voellmy-type models were tried to back-

* *Corresponding author address:*
David Hamre, David Hamre and Associates, LLC, Alaska, USA
tel: +1-907-223-9590
email: davidhamreassociates@gmail.com

calculate known slushflow events (e.g., Gauer, 2016; Skred, 2021). The observations from 1982, along with more recent work, are important to developing appropriate slushflow models.

2. OBSERVATIONS

Using a strategy of defining contributory factors, the team in 1981/82 developed a working theory about what it took to create a slushflow. Atigun Pass typically sees slushflows from low angle gullies in large drainage basins. These gullies are confined and are likely created or modified by slushflows.

2.1 Climate Factors

Winters in the Brooks Range are long and cold. Persistent temperatures of -30 to -40°C occur. The basins above slushflow gullies typically have a shallow snowpack throughout the winter. Sustained winds are common, blowing the shallow snow around and sintering it into small crystals. This wind-borne snow tends to collect to greater depths only in low angle gullies, which are better protected from wind. Due to consistently cold temperatures and shallow snow, the snowpack tends to be very cold and faceted except in the deeper gullies. These cold temperatures are maintained at the snow/ground interface late into the spring. Temperatures on north facing slopes on the ground surface on June 1 of -10°C have been recorded. Few or no water channels develop in the snowpack at these temperatures.

The springtime meltdown begins in earnest when the sun comes above the horizon 24 hours per day, typically on May 26. When the thaw boundary reaches Atigun Pass (Latitude 68° North), the snowpack warms quickly from the surface downwards (Hamre and Stethem, 1980).

2.2 Water Generation

During this spring meltdown, free water is generated quickly, assisted by the sprinkling of dark rocks exposed in basins with shallow snowpacks, which generate heat. Large alpine basins pour this generated water quickly through a porous, faceted snowpack downhill, where the water intercepts a different snowpack in the low angle gullies that form slushflows. Here, the much deeper snowpack consists primarily of tightly packed, wind-blown snow that impedes the transmission of liquid water. As the melt progresses, water in these gullies continues to rise until it reaches the surface. This timing is shown by a blue ribbon of free-flowing water on the surface, which is indicative that the gully is now primed for a slushflow event (Figure 2). This progression is similar to what was described by Hestnes et al. (2012).

Figure 2: Snowpack primed for release near Atigun Pass (Photo: Courtesy of A.P.S.C.)

2.3 Release Mechanisms

Little is known about the actual trigger mechanism required for slushflows. Most occur naturally when the water input is much higher than the pore space allows for escapement. Alternatively, a rain event might rapidly overload low angle gullies. Slushflows may be a phenomenon that will happen more frequently in temperate snow climates in the future, with higher elevation and heavier rain events. On rare occasions, a wet snow event from steeper slopes above may trigger a slushflow. (Jaedicke et al., 2012, Fig. 4.2). This condition was observed in the early 1980s when the only observation of a triggered slushflow event at Atigun Pass occurred. It was triggered by a wet slab avalanche that was artificially triggered. This wet snow avalanche traveled down the north face of Clealand Peak to the upper reaches of Sheep Gully, where it triggered an observed slushflow (Figure 3).

Figure 3: Avalanche (green) Triggered Slushflow (yellow) in Sheep Gully (Photo: Courtesy of Earth Analytics)

2.4 Flow Mechanisms

As the wet slide (Sect. 2.3) came to a stop, a slab was observed to fracture and change color. Changing from a consistent white color to a steely

gray color, the slushflow accelerated downhill and quickly assumed a large lobate, teardrop shape. The teardrop was tapered in the rear. It traveled down the gully for a distance of almost 2 km. The flowing material maintained a teardrop shape throughout and did not change to a turbulent flow, reaching a steady state in size within approximately 5 seconds of releasing. Since the flowing material (teardrop) entrains rocks, slush, and virtually anything in its path but reaches a stable form, intuitively, it also must be discharging material. The observations indicate this discharge was in the form of disaggregated water, which transitioned to turbulent flow, likely because of a phase change during the disaggregation process.

2.5. Fracture Angle and Depth

During both the 1981 and 1982 seasons, numerous slushflows were observed, and pertinent information was gathered, as presented in Table 1.

Table 1: Observed slushflow parameters (Courtesy of A.P.S.C.). H is thickness of the fracture, W the width of the crown, L Crown-to-Stauchwall distance, Θ angle from the horizontal at crown, α mean slope of path, ρ mean snow density in crown.

Name	Date	H (m)	W (m)	L (m)	Θ (°)	α (°)	ρ (kg/m^3)
Bear Valley #2	5/18/81	3.0	12	50	17	12	–
Bear Valley #1	5/18/81	3.3	14	–	15	9	–
Sluice Box	5/26/81	4.0	12	50	10	15	610
Sheep Chute	5/16/81	1.5	10	–	10	9	–
Grizzly Gulch	5/26/81	2.7	13	–	15	10	600
No Name	5/26/81	1.2	7	–	18	–	600
Bear Valley #1	6/6/82	5.3	13	–	17	7	630
Grand Whaleback	6/6/82	4.8	16	50	17	9	630
Sluice Box	6/6/82	6.6	18	–	21	10	590

The steepest release angle noted was 21 degrees with the average closer to 15 degrees. Snowpack densities after the release of water saturated snow (>600 kg/m^3) are also high.

2.6. Runout Characteristics

As the teardrop shaped event exits confined gullies and enters a distinct runout zone, the flow material disaggregates into water, snow, and rock. Figure 4 shows the resulting snow deposit from Waterfall Gully onto the road.

Figure 4: Disaggregated snow from Waterfall Gully on the Dalton Highway (Photo: Courtesy of R. Bahnson)

The slushflow event that is narratively described came from Sheep Gully (Figure 5), where the residual fracture line is seen.

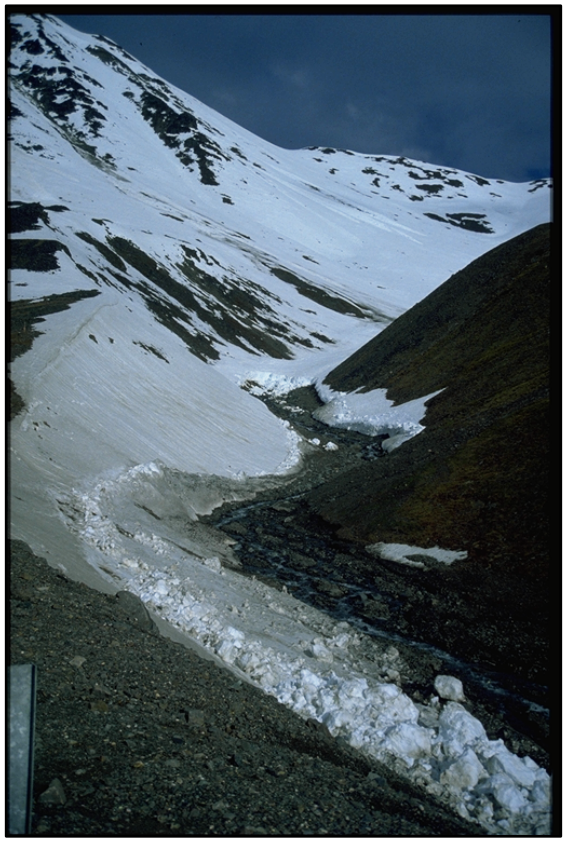

Figure 5: Slushflow from Sheep Gully. Fracture and track. The superelevation of the flow is obvious. (Photo: Courtesy of R. Bahnson)

Disaggregated water, besides responding as described in Sect. 2.4, is released to run down the watercourse as the event ends in a turbulent flow. Because there is a high level of rock debris entrained in the flowing material, large depositions of rock result in the runout zone. Where this material intersects a building or roadway, it leaves behind a rocky deposit, as shown in Figure 6.

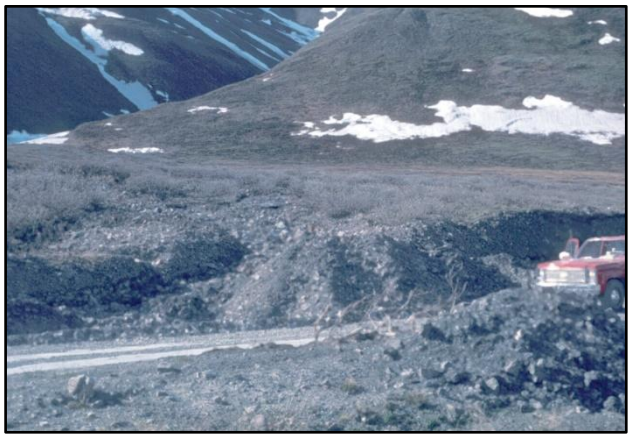

Figure 6: Disaggregated rock debris on the Dalton Highway (Photo: D. Hamre)

These rocky deposits commonly result in a geologic feature known as a "whaleback," which is very distinctive. They form at the bottom of virtually every slushflow gully in the Brooks Range (Figure 7).

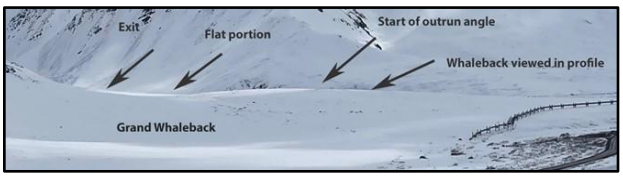

Figure 7: Grand Whaleback (Photo: Courtesy of G. Scott)

Because this rock material is turned over in the slushflow, lichens are removed. Thus, rock deposits can be dated with lichen growth analysis (Calkin and Ellis, 1980). While the lichen work is helpful in establishing the age of deposits, it likely cannot be used for establishing frequency/magnitude relationships other than very coarse ones.

2.5 *Risk Analysis*

Slushflows typically produce a low Avalanche Hazard Index (AHI) (Schaerer, 1979) value on the road over Atigun Pass. The calculated Q Factor or impact force is very high, but their low frequency is the reason behind a low AHI. It is nevertheless important not to put facilities in the way of slushflow runout, as shown in recent examples (Hestnes and Kristensen, 2010). Diversion dikes are effective for channelizing slushflows as long as the angle change of the flow is shallow and material (rock) storage is cleaned out.

3. MODELING

3.1 *General-flow models available, the challenge of 3D modeling, phase change challenges with a model.*

Presently, there are no operational models available that were developed specifically for slushflows. Bozhinskiy and Nazarov (1998) presented a two-layer model for slushflows and tested it under idealized conditions in a uniform channel. Kobayashi and Izumi (1989) did some rheological testing on the behavior of slush. They found a non-Newtonian relationship between viscosity and shear rate and found that effective viscosity decreases with an increasing ratio of water/snow content (W/S). They measured an effective viscosity of the order O(1-60 Pa·s). As long as W/S stays constant, slushflows might be regarded as a simple non-Newtonian fluid. However, this is probably not always valid, especially in the runout area where water starts to detrain, and a multiphase model would be more appropriate but far more complicated. In this study, we restrict ourselves to two single phase approaches. The first is based on a common depth-averaged model, and the second one is on a fully 3D MPM method.

3.2 *Depth-averaged Model*

The depth-averaged model uses a kind of blending rheological model based on a Bingham-Coulomb type model (cf. Chen and Lee, 2002):

$$\left(\sigma_{xz}^{b}, \sigma_{yz}^{b}\right) = \frac{\boldsymbol{u}}{\|\boldsymbol{u}\|}\left[3M_b\frac{\|\boldsymbol{u}\|}{h} + 1.5\tau_y + \mu_e\bar{\sigma}_{zz}\right] \qquad (1)$$

where M_b is the Bingham viscosity, τ_y the shear strength, μ_e is an effective Coulomb-friction factor, and $\bar{\sigma}_{zz}$ is the slope normal stress. It is assumed that the effective Coulomb friction factor depends on the pore water pressure. However, as we deal with a single phase model, it is assumed to stay constant during the whole flow. The model is implemented in the SAMOS-solver (Sampl and Granig, 2009), which allows, to a certain degree, one to define one's own bottom friction.

Table 2: Initial mass and parameter used. In addition, the normalized travel time of the simulation is given. In all cases, the maximum available erosion mass was set at 250 kg m^{-2}.

Path	mass (10^6 kg)	M_b (Pa·s)	τ_y (Pa)	μ_e (-)	$\frac{t_{sim}}{\sqrt{\frac{S_{sim}}{g\,sin\alpha}}}$ (-)
Bear Valley	2.6	3	100	0.1	2.5
Slush Gully	2.7	2	100	0.075	3.9
Grand Whaleback	3.3	3	100	0.1	2.7

Figure 8 shows examples of the simulated maximum velocity along the tracks, as shown in Table 2.

The maximum velocity in the case of the Bear Valley simulation is 27 m s^{-1}. This is in accordance with

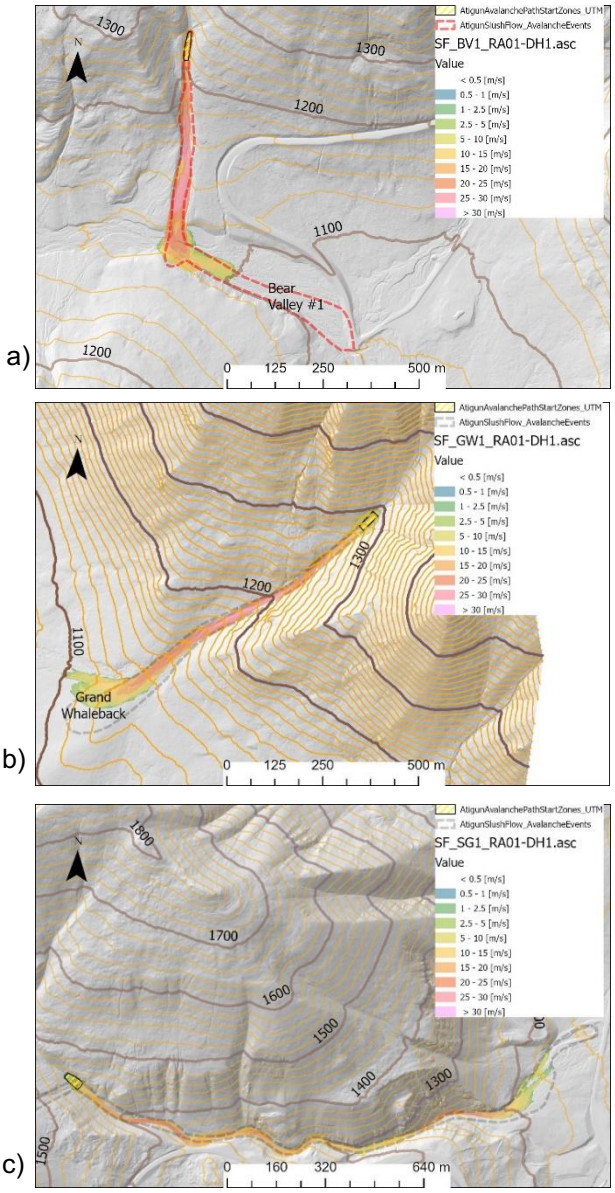

Figure 8: Maximum velocity: a) Bear Valley, b) Grand Whaleback c) Sheep Gully.

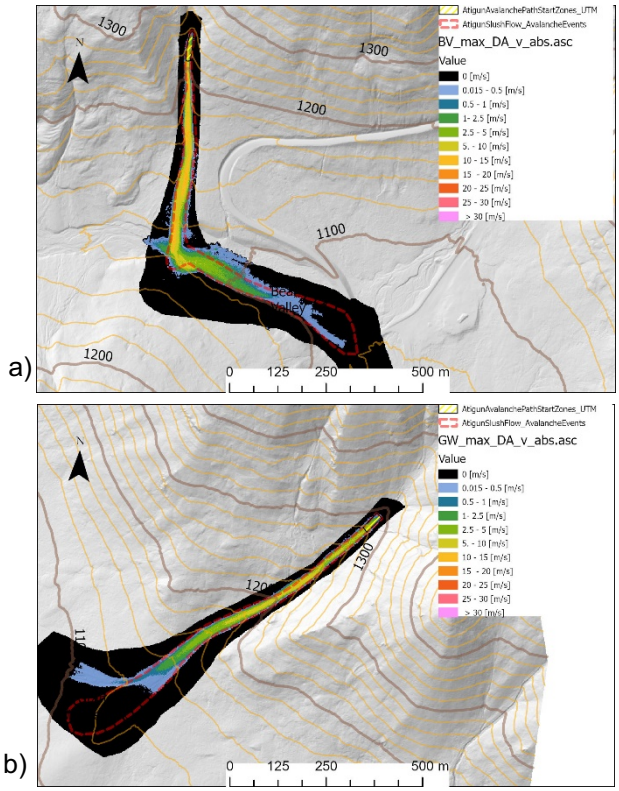

Figure 9: Maximum depth-averaged velocity in the 3-D MPM simulations: a) Bear Valley, b) Grand Whaleback. The black background highlights the erodible layer, which is explicitly simulated.

estimates of 25 m s^{-1} by Art Mears based on runup calculations. The simulated normalized travel time,

$$\frac{t_{sim}}{\sqrt{\frac{S_{sim}}{g\,\sin\alpha}}} \qquad (2)$$

which is shown in Table 2, agrees with collected observations from other locations (Gauer, 2020). Here, the travel time t_{sim} and travel distance S_{sim} are proxies for the more mobile part of the flow, not including possible creep at the end–basically, it is what an observer would report as a first guess. The Bear Valley and the Sheep Gully simulation seem to run too short. This might be attributed to the fact that the model cannot reproduce the water drain out common in the runout area. In the Sheep Gully simulation, similar meandering behavior can be seen as in the observations (cf. Fig. 5). In the Grand Whaleback simulation, the model tends to follow the steepest gradient, as one would expect. That the observation shows a more straight direction could suggest even higher inertia in the real flow or an effect from self-channelization, which is not accounted for in the 2D model–or a combination of both.

3.3 *Three-dimensional MPM model*

The Material Point Method (MPM) is used to conduct fully three-dimensional modeling of these events. This numerical continuum scheme is chosen due to its ability to handle large deformation of elasto-plastic materials combined with its easy handling of complex terrain (Gaume et al. 2018; Li et al. 2021; Kyburz et al. 2024) and entrainment (Li et al. 2022). Similarly to the depth-averaged approach outlined above, a Bingham-Coulomb-like model is used. More precisely, a Drucker-Prager yield criterion $\tau_y = \mu p + \tau_c$ determines the onset of plastic deformations and the shear strain rate is given by

$$\dot{\gamma}_s = \frac{1}{t_{visc}} \frac{\tau - \tau_y}{\tau_y} \qquad (3)$$

where μ is the Coulomb-friction factor, τ_c determines the cohesion and t_{visc}= 0.2 s is the viscous time used

in all simulations. See Blatny et al. (2023) for more details about the elasto-viscoplastic implementation.

An erodible and initially cohesive layer of 3 m with $\tau_c = 50$ kPa covers the terrain, and the cohesionless release zones are placed on top of this layer. Once the erodible layer yields due to the force exerted by the flowing material, its cohesion τ_c is set to 0, thus promoting entrainment. The density of both the erodible layer and the release zones is 630 kg/m^3, using in all cases a Young's modulus of 1 MPa and a Poisson's ratio of 0.3. As the observations suggest a smaller friction in Bear Valley, μ = 0.05 is used here compared to 0.13 in Grand Whaleback. The results are shown in Figure 9, which also highlights the erodible layer as the black background color.

In the Bear Valley scenario, the maximum depth-averaged velocity reaches approximately 15 m/s. For the Grand Whaleback simulation, this value is slightly lower at around 10 m/s. The runout distance in Bear Valley is relatively well reproduced, although we observe more splashing at the bottom of the slope and after the turn due to superelevation effects. In the Grand Whaleback case, the MPM simulation, similar to the depth-averaged model, diverges from the observed runout path, which shows a rather unphysical tendency to ascend a minor topographic rise. It is important to note that while the velocity values derived from depth-averaging the 3D results appear relatively low, the maximum velocity observed at the flow surface can be approximately twice as high as the depth-averaged value. In more detail, in the Bear Valley case, the maximum 3D velocity is slightly above 25 m/s, while in the Grand Whaleback case, it reaches around 20 m/s. This discrepancy suggests that the depth-averaged velocities may underestimate the peak surface velocities, potentially leading to a better alignment with the observations reported by Art Mears if surface velocities are considered.

4. DISCUSSION

In this paper, we present observations of slushflows and apply two distinct modeling approaches as an initial attempt to reproduce these events. The first approach employs a depth-averaged model using SAMOS, a Lagrangian finite-volume solver, based on a Bingham-Coulomb rheology. The second approach utilizes a three-dimensional model based on the Material Point Method (MPM), a hybrid Eulerian-Lagrangian technique, incorporating a similar rheological model within an elasto-viscoplastic framework. In the depth-averaged model, the key adjustable parameters include Coulomb friction, viscosity, shear strength, and maximum entrained mass. Similarly, the 3D model allows for adjustments to friction, viscosity, strength, and erodible bed height, along with elastic properties, though the latter has a minimal impact in this context. The parameters for both models were independently adjusted to best match the observations. While the friction parameters were found to be similar, the viscosity values differed significantly by an order of magnitude. The viscosity used in the MPM simulation falls within the upper range of values reported by Kobayashi and Izumi (1989), whereas the depth-averaged model employed a viscosity from the lower range. This discrepancy in viscosity and the fact that the maximum velocities differ from the depth-averaged ones in the MPM model (discussed in Section 3) likely contribute to the observed differences in velocity between the two modeling approaches. For future studies, a direct comparison using similar input parameters would be beneficial.

It is also important to highlight the significant difference in computational time between 2D depth-averaged (DA) and 3D depth-resolved methods. While DA model simulations typically run in a couple of minutes, 3D simulations require several hours. This discrepancy arises primarily because the MPM model explicitly simulates the entire erodible snowpack, which can be over ten times larger in volume than the release zone. To reduce computational costs, future work should explore alternative strategies for simulating entrainment in 3D. On the other side, simulating for the whole erodible snowpack accounts explicitly for self-channelization, which is a common feature in slushflow events.

Finally, although both simulation techniques yield promising and encouraging results, they fall short in capturing the multiphase nature of slushflows, where water and snow can move at significantly different velocities, particularly near the bottom of the slope. Moving forward, it will be essential to develop or apply two-phase models, whether depth-averaged or 3D, to more accurately simulate slushflows.

5. CONCLUSIONS

In this paper, we present some slushflow observations from Alaska. These observations provided the starting point for a feasibility study of two modeling approaches, namely a 2D depth integrated model based on a Bingham-Coulomb type base friction and a fully 3D MPM model using Drucker-Prager rheology. Although the simulations show overall reasonable results, it is clear that variable flow stages, commonly present in slushflows, can hardly be reproduced with a single-phase approach.

Recent advancements in modeling capabilities have allowed for adaptations that might include multiphase processes (e.g., Pastor et al. 2018) in the future for events like slushflows. The key observations that were privately held from the 1982 research project assist with model development by identifying

constraining characteristics. These kinds of observations are important to better understand the flow behavior, which is necessary to improve modeling capabilities for slushflows.

ACKNOWLEDGEMENT

The authors thank Alyeska Pipeline Service Company for allowing the information generated by the 1982 study to be published. We also thank Reid Bahnson for permission to use his photographs and for his many years of observations in Atigun Pass.

REFERENCES

Blatny, L., Modeling the mechanics and rheology of porous and granular media: an elastoplastic continuum approach. PhD thesis, No. 10267. EPFL, 2023.

Bozhinskiy, A. N., Nazarov, N. N., Dynamics of two-layer slushflows. Hestnes, E. (Ed.) 25 Years of Snow Avalanche Research at NGI, Anniversary Conference, Voss, Norway, 12-16 May 1998, Proceedings, Vol. 203 NGI Publ.: Oslo p. 74-78,1998

Calkin, P. E., Ellis, J. M., A Lichenometric Dating Curve and its Application to Holocene Glacier Studies in the Central Brooks Range, Alaska Arctic and Alpine Research, Vol. 12, No. 3 p. 245-264 Hestnes, E. / Kristensen, K. (2010) The diversities of large slushflows illustrated by selected cases, Proceedings of the International Snow Science Workshop, Lake Tahoe, CA, 2010 p. 348-355, 1980

Chen, H. and Lee, C. F. Runout analysis of slurry flows with Bingham model, Journal of Geotechnical and Geoenvironmental Engineering, 2002, 128, 1032-1042, 2002

Gauer, P., Numerical modeling of a slushflow event, Proceedings of the International Snow Science Workshop 2004, Jackson Hole, Wyoming, United States p. 39-43, 2004

Gauer, P., Results 2015 from SP 4 FoU Snøskred: Work Package 3 Deliverable D3.4 Back-calculations of slushflow events, 20140053_Årsrapport_2016_WP3, Norwegian Geotechnical Institute, 2016

Gauer, P. (2020) SP 4 FoU Snøskred: Annual Report 2019 WP 3 Deliverable D3.2 Collection of observed slushflow velocities, NGI report 20170131-17-R, Norwegian Geotechnical Institute, 2020

Gaume J., Gast T., Teran J., van Herwijnen A., Jiang C. Dynamic anticrack propagation in snow. Nature Communications 9, 3047, 2018.

Hamre, D., Stehem, C. J., Temperature Based Forecasting of a Springtime Arctic Snowpack Proceedings of the 1980 International Snow Science Workshop, Vancouver, BC, Canada Pp. 82-89, 1980

Hestnes, E., Kristensen, K., Bakkehøi, S., Slushflows - a challenging problem to authorities and experts, Juras, R. (Ed.) IV International Conference "Avalanches and Related Subjects" Kirovsk, Russia September 5 - 9, 2011

Hestnes, E., Bakkehøi, S., Kristensen, K., Slushflow formation, flow regimes and consequences (short version), Proceedings of International Snow Science Workshop 2012, September 16-21, at the Dena'ina Center in Anchorage, Alaska, pp. 414-419, 2012

Hestnes, E., Jaedicke, C., Global Warming Reduces the Consequences of Snow-related Hazards Proceedings of the International Snow Science Workshop 2018, Innsbruck, Austria, pp. 493—497, 2018

Jaedicke C., Hestnes E., Høydal, Ø.A., A review on Slushflows, 20120096-01-R Norwegian Geotechnical Institute, 2012

Kobayashi, S., Izumi, K., Viscosity of Slush First International Conference on Snow Engineering, Santa-Barbara, California, July 1988, Vol. CRREL, Special Report 89-6, February 1989 p. 346-353, 1989

Mears, A. Release and Motion of Arctic Slushflows, Proceedings of the 1982 International Snow Science Workshop, Bozeman, Montana, USA, pp. 3-4, 1982

Onesti, Slushflow/slush avalanche terminology, ICE News Bulletin of the International Glaciological Society, Number 107, Issue I, p. 20, 1995

Pastor, M., Yague, A., Stickle, M. M., Manzanal, D., & Mira, P. A two-phase SPH model for debris flow propagation. International Journal for Numerical and Analytical Methods in Geomechanics, *42*(3), 418-448, 2018

Palsson, H., Helgadottir, A., Jones, R. A., The design of slushflow barriers: OpenFOAM simulations 2019 International Symposium on Mitigative Measures against Snow Avalanches and Other Rapid Gravity Mass Flows, Siglufjördur, Iceland, April 3–5, 2019

Sampl, P., Granig, M. Avalanche Simulation with SAMOS-AT Proceedings of the International Snow Science Workshop, Davos p. 519-523, 2009

Skred, A.S, Bruk av RAMMS:DEBRISFLOW på kjentesørpeskredhendelser 2021, No. 9/2011 Norges vassdrags- og energidirektorat (NVE), 2021

Tómasson, G. G., Hestnes, E., Slushflow hazard and mitigation in Vesturbyggd, Northwest Iceland 2000 Nordic Hydrology, Vol. 31, No. 4-5 p. 399-410, 2000